Journal of Plant Physiology 279 (2022) 153839

Contents lists available at ScienceDirect

Journal of Plant Physiology

journal homepage: www.elsevier.com/locate/jplph

Increased levels of cell wall degrading enzymes and peptidases are associated with aggressiveness in a virulent isolate of *Pyrenophora teres* f. *maculata*

Mahmut Emir [a], Ahmet Caglar Ozketen [b], Ayse Andac Ozketen [c], Arzu Çelik Oğuz [d], Mei Huang [e], Aziz Karakaya [d], Christof Rampitsch [e,**], Aslihan Gunel [a,*]

[a] Kirsehir-Ahi Evran University, Faculty of Arts and Sciences, Department of Chemistry, Kirsehir, Turkey
[b] Middle East Technical University, Department of Chemistry, Ankara, Turkey
[c] Basic Sciences Unit, TED University, Ankara, Turkey
[d] Ankara University Faculty of Agriculture, Department of Plant Protection, Dışkapı, Ankara, Turkey
[e] Agriculture and Agrifood Canada, Morden Research and Development Centre, Morden MB, Canada

ARTICLE INFO

Keywords:
Pyrenophora teres f. maculata
secretome
spot form of net blotch disease

ABSTRACT

Pyrenophora teres f. *maculata* (*Ptm*) is a fungal pathogen that causes the spot form of net blotch on barley and leads to economic losses in many of the world's barley-growing regions. Isolates of *Ptm* exhibit varying levels of aggressiveness that result in quantifiable changes in the severity of the disease. Previous research on plant-pathogen interactions has shown that such divergence is reflected in the proteome and secretome of the pathogen, with certain classes of proteins more prominent in aggressive isolates. Here we have made a detailed comparative analysis of the secretomes of two *Ptm* isolates, GPS79 and E35 (highly and mildly aggressive, respectively) using a proteomics-based approach. The secretomes were obtained *in vitro* using media amended with barley leaf sections. Secreted proteins therein were harvested, digested with trypsin, and fractionated offline by HPLC prior to LC-MS in a high-resolution instrument to obtain deep coverage of the proteome. The subsequent analysis used a label-free quantitative proteomics approach with relative quantification of proteins based on precursor ion intensities. A total of 1175 proteins were identified, 931 from *Ptm* and 244 from barley. Further analysis revealed 160 differentially abundant proteins with at least a two-fold abundance difference between the isolates, with the most enriched in the aggressive GPS79 secretome. These proteins were mainly cell-wall (carbohydrate) degrading enzymes and peptidases, with some oxidoreductases and other pathogenesis-related proteins also identified, suggesting that aggressiveness is associated with an improved ability of GPS79 to overcome cell wall barriers and neutralize host defense responses.

1. Introduction

Net blotch, caused by *Pyrenophora teres* Drechsler [anamorph: *Drechslera teres* (Sacc.) Shoem.] is an economically important leaf disease of barley, with yield losses accounting for 10–40% of the harvest in all barley-growing regions (Çelik Oğuz and Karakaya, 2017; Mathre, 1997; Wyatt and Friesen, 2021). The causative fungus has two different forms, presenting two different symptoms of net blotch. These are the spot form of net blotch (SFNB), caused by *P. teres* f. *maculata,* (*Ptm*), and the net form of net blotch (NFNB), caused by *P. teres* f. *teres* (*Ptt*). SFNB was first described in Denmark in the 1960s (Smedegård-Petersen, 1977). Its symptoms include a chlorotic halo and oval necrotic lesions on the leaves of infected plants. By contrast, NFNB presents necrotic mesh-like patterns (nets) and striated lesions (Smedegård-Petersen, 1977). Although *Ptt* and *Ptm* are morphologically indistinguishable, host-pathogen interactions are not identical. Both form germ tubes and appressoria, however, *Ptt* directly enters the epidermal cells while *Ptm* at first forms haustoria-like vesicles and acts as a biotroph before rapidly switching to a necrotrophic growth phase – *Ptm*, thus has a more hemibiotrophic growth habit (Lightfoot and Able, 2010). Some researchers have argued that although the two forms of *P. teres* are found in the same field and may indeed infect the same leaf, they should be classified as

* Corresponding author.
** Corresponding author.
E-mail addresses: Chris.Rampitsch@agr.gc.ca (C. Rampitsch), agunel@ahievran.edu.tr, gunel.aslihan@gmail.com (A. Gunel).

https://doi.org/10.1016/j.jplph.2022.153839
Received 26 March 2022; Received in revised form 22 September 2022; Accepted 7 October 2022
Available online 1 November 2022

separate species based on their genome sequences and the rarity of hybridization between the two forms in nature (Clare et al., 2020; Ellwood et al., 2012; Jalli, 2011; Rau et al., 2007; Syme et al., 2018). Both forms of the pathogen secrete molecules either to manipulate the host or to supply their foods from the environment. These range from small molecules such as phytotoxic pyrenolines and pyrenolides (Coval et al., 1990; Nukina et al., 1980), to peptide alkaloids (Bach et al., 1979). The latter especially cause chlorosis, and Sarpeleh et al. (2007) demonstrated that peptides act as effectors which contribute to symptoms of the net blotch in barley cultivars in Australia.

SFNB is gaining prominence in major barley-producing regions of the world (Lartey et al., 2013; Liu et al., 2011; McLean et al., 2014) as it decreases grain size, density, and filling rate as well as lowers feed and malt quality (Liu et al., 2011; Wang et al., 2015). While genetic and genomic approaches have identified pathogenicity QTL (Jalli, 2011; Rau et al., 2007; Syme et al., 2018) and histological studies of the development of this fungus *in planta* describe the infection process (Smedegård-Petersen, 1977), the underlying molecular interactions between *P. teres* and barley remain largely unknown.

Virulent isolates of *Ptm* exhibit different levels of aggressiveness – i.e. they can cause SFNB with different levels of severity (Karakaya and Akyol, 2006; Gerlegiz et al., 2014; Usta et al., 2014), a phenomenon commonly observed with other plant pathogens (Pariaud et al., 2009). Secreted proteins likely play key roles in determining aggressiveness as they do in *Fusarium graminearum* (Fabre et al., 2019), *Clavibacter nebraskensis* (Soliman et al., 2021), and *Magnaporthe oryzae* (Liu et al., 2022; Zhao et al., 2021). In these studies, the content of the secretomes revealed potentially important ingredients of aggressiveness. Some of these proteins were enzymes with known functions, for example with cell-wall degrading abilities, others were putative effector candidates without known functions (Demirci et al., 2016). It has been proposed that under nutrient stress conditions, such as a lack of N and C, the abundance of cell wall degrading enzymes (CWDEs) and glycosyl hydrolase proteins is tightly regulated (Oh et al., 2017; Nitsche et al., 2012). Furthermore, increasing CWDEs in the presence of different carbon sources for fungal growth has been linked to pathogen virulence (Wang et al., 2011).

Fungal phytopathogens deploy varying sets of secreted effectors to facilitate nutrient uptake, fine-tune their adaptation to environmental conditions, and interact with the host to modify defense layers (Bahram and Netherway, 2022). Among these, the proteinaceous secretome is informative to study the isolate-specific behavior of plant pathogenic fungi and deciphering the susceptibility and resistance mechanisms (Bradshaw et al., 2021). There are several reports published that list and characterize the secretomes of *Ptt* using either proteomics, transcriptomics, or genomics strategies (Ismail and Able, 2016; Muria-Gonzalez et al., 2020; Wyatt et al., 2018). In the *Ptt* secretome study conducted by Ismail and Able (2016), gel-based approaches were used to examine 7 isolates with different levels of aggressiveness. They identified a total of 259 proteins of which 202 could only be assigned functional domains. This group had also previously compared an aggressive (32/98) and mild (08/08f) isolate of *Ptt* with the aim of identifying virulence-related proteins; the authors reported on three of these – PttXyn11A, PttCHFP1, and PttSP1 from the aggressive isolate (Ismail et al., 2014). However, there are no corresponding reports from the *Ptm* secretome.

Here we have compared the secretomes of an aggressive and a mild isolate of *Ptm* grown *in vitro* in the presence of detached barley leaves using a label-free quantitative proteomics approach, with relative quantification of proteins based on precursor ion intensities. We have demonstrated that the secretome of an aggressive *Ptm* isolate is enriched mainly in cell wall-degrading enzymes, peptidases, and pathogenesis-related proteins. Furthermore, we have predicted that a candidate effector (PTMSG1_04452) from identified proteins bears the necrosis-inducing *Phytophthora* protein 1 (NPP1) domain. PTMSG1_04452 (*Ptm*NPP1) induces cell death in *Nicotiana benthamiana* leaves, and the observed cell death is delayed if the signal peptide is removed. The finding indicates the *Ptm* secretome contains secreted candidate effector proteins that trigger cell death response *in planta*.

2. Materials and methods

2.1. Biological materials

The aggressive GPS79 and less aggressive E35 isolates of *Ptm* were collected from barley (*Hordeum vulgare* L.) fields in Central Anatolia, Turkey. To determine their aggressiveness on barley, they were inoculated onto three plants of the susceptible cultivar 'Bülbül 89' and rated after seven days. Inoculation, incubation, and disease assessment procedures were the same as described by Çelik Oğuz and Karakaya (2017).

2.2. Growth of isolates

GPS79 and E35 *Ptm* isolates were grown on Potato Dextrose Agar (PDA) for 10 days in an 8h dark/16 h day cycle at 23 °C. On the seventh day, 10 mycelia plugs with a 5 mm radius of each isolate were transferred to glass bottles containing 1-L Potato Dextrose Broth (PDB) supplemented with ten 5 cm leaf sections of 'Bülbül 89' barley. Before addition to the broth, barley leaves (Zadoks growth stage 13) (Zadoks et al., 1974) were surface sterilized for 2 min with 2% NaOCl and rinsed three times with sterile distilled water under aseptic conditions. Bottles containing isolates and barley leaves were grown on a shaker rotating at 250 RPM for 7 days in an 8h dark/16 h day cycle at 23 °C.

2.3. Protein extraction

All chemicals used were purchased from Merck, Sigma, or ThermoFisher Scientific. Five independent biological replicates were prepared for each isolate. PDB was filtered through filter paper under a vacuum and the filtrate, containing secreted proteins, was collected on ice. Secreted proteins were precipitated by adding 4 vol of ice-cold acetone containing 10% (w/v) trichloroacetic acid (TCA) (w/v) and 0.07% (w/v) dithiothreitol (DTT). The mixture was briefly vortexed and kept at −20 °C overnight. Protein extracts were centrifuged at 12,000 *g* for 20 min at 4 °C. The resulting pellet was washed four times with cold acetone containing 0.07% (w/v) DTT. After the last wash the pellet was dried and dissolved in RIPA buffer (150 mM NaCl, 50 mM Tris.HCl pH 8.0, 1% (w/v) NP-40, 0.5% (w/v) sodium deoxycholate, 0.1% (w/v) SDS) containing protease and phosphatase inhibitor cocktails, before being sonicated 5 times for 30 s with 5 intervals in an ice bath. The final suspension was clarified by centrifugation, 30 min 30,000 *g*, 4 °C, and the supernatant was divided into aliquots and stored at −80 °C (Rampitsch et al., 2006). Protein concentration was measured using the BCA assay with BSA as the standard (Smith et al., 1985).

2.4. In solution protein digestion

Before digestion, samples containing 500 µg protein were reduced in 5 mM DTT for 1 h at room temperature and alkylated by adding 50 mM iodoacetamide at room temperature in the dark for 50 min. Alkylated proteins were precipitated by adding 4 vol of methanol to the samples, vortexing briefly, and then adding 1 volume of chloroform and vortexing again. Water was then added (3 vol) until a milky appearance formed. The phases were separated by centrifugation, 20,000 *g* 10 min. Three phases were formed following centrifugation and protein from the interphase was harvested. The protein pellet was washed with methanol and centrifuged as previously to collect the protein pellet. The pellet was retained and dried and then dissolved in 50 mM Tris.HCl pH8.5 containing 8 M urea. After dissolving as much protein as possible the urea was diluted to 1 M with 50 mM Tris.HCl pH8.5. Proteins were digested with trypsin/Lys-C (100:1, w/w) using conditions and buffers recommended by the manufacturer (Promega). After the digestion, the

reaction was quenched with 0.5% (v/v) trifluoroacetic acid (TFA). Peptide desalting was performed by using a C_{18} sepPak column and dried using a Speed Vac (Saei et al., 2019).

2.5. Off-line separation of peptides by RP-HPLC

Peptides were resuspended in 2 ml 10 mM NH_4OH, pH 10, and fractionated by Reversed Phase HPLC (Dwivedi et al., 2008). A C_{18} column (Waters: Xbridge BEH C18 250 × 4.6 mm, 5 μm particles) and an analytical HPLC unit (Ultimate 300: Dionex/ThermoFisher Scientific, Bremen, Germany) were used. A gradient of pure mobile phase A (10 mM NH_4OH, pH 10) to 60% mobile phase B (A in 80% (v/v) ACN) was delivered at 0.5 ml min^{-1}. The absorbance of the eluant was monitored at 280 nm and thirty 0.5 ml fractions were collected throughout. The first 9 ml were discarded, and the remainder were pooled in sets of three by combining every tenth fraction. Pooled fractions were dried in a speed-vac and stored at −20 °C until required. Thus, each experimental group (i.e., biological replicates of either E35 or GPS79) contained 18–20 fractions for a total of 74 from E35 and 99 from GPS79. Although the yield of the second biological replicate of E35 was low, each isolate yielded at least four good biological replicates, and a total of 173 samples were injected into the LC-MS, resulting in 173.RAW files to be queried.

2.6. Mass spectrometry

Pooled fractions were re-dissolved in 20 μl of mobile phase A1 (water containing 2% (v/v) ACN and 0.1% (v/v) FA). All four biological replicates were analyzed in a single session. Tryptic peptides were separated through a C_{18} column (19 cm fused silica column, 75 μm ID, packed with Vydac C18, 5 μm beads, 300 Å pores) coupled directly to the mass spectrometer via a nanoelectrospray ionization source. An acetonitrile gradient of mobile phase A1 to 50% mobile phase B1 (0.1% (v/v) FA in ACN) was delivered at 300 nl/min over 60 min (Easy nLC1000: ThermoFisher Scientific, San Jose CA), with a total program length of 120 min. Mass spectra were acquired in a hybrid quadrupole-Orbitrap mass spectrometer (Q-Exactive: ThermoFisher Scientific, Bremen, Germany). A survey scan acquired over the range m/z 300–2000 was followed by 12 MS^2 scans of the most intense ions, with dynamic exclusion set to 15 s.

2.7. Data analysis

Simultaneous protein identification and label-free quantification (LFQ) were performed using MaxQuant (v1.6). The search parameters were mostly left at default settings. Briefly, these were, monoisotopic mass accuracy of ±20 ppm for the first search and ±4.5 ppm for the second; up to two missed cleavages for tryptic peptides; peptide charge up to +7; fixed modification of carbamidomethyl (Cys), and variable modification of oxidation (Met) and acetylation (N-terminus). Raw MS data files were queried against the genomic sequences of *P. teres* f. *maculata* (10,621 sequences, UniProt). The genomic database of *P. teres* f. *maculata*, registered to NCBI in 2020 and downloaded on 3rd June 2021, was used. The isolate names are P-A14, FGOB10Ptm-1, NZKF2, and DEN2.6 respectively (Mayer et al., 2012). The genomic database for *Hordeum vulgare* (236,301 sequences) was downloaded from the International Barley Sequencing Consortium in May 2021 (Hordeum_vulgare.IBSC_v2.pep.all.fasta from http://plants.ensembl.org/Hordeum_vulgare/Info/Index) (International Barley Genome Sequencing Consortium, 2012). The search was set up so that analogous fractions among biological replicates were treated as identical, and that peaks from neighboring fractions could be used to generate quantitative data.

The results generated from MaxQuant were analyzed using Perseus (v1.6), which is companion software to MaxQuant used for statistical analysis. The LFQ values generated by MaxQuant were loaded as main columns for statistical analyses. The matrix was then reduced by filtering out proteins only identified by site, potential contaminants (from the default list of common contaminants embedded in the software), and proteins with a reversed sequence (decoys). The intensity values were transformed logarithmically (log_2) and rows were filtered based on valid values, with at least two required per row, i.e. each identified peptide had to have a valid LFQ value in at least two biological replicates to be included in the final data. In cases where LFQ values were missing, the missing value was imputed using random numbers generated from the Gaussian distribution of the existing values, but down-shifted by 1.8 standard deviations (width set to 0.5 SD) to mimic low abundance protein LFQ values more accurately, as described by Tyanova and colleagues (Tyanova et al., 2016). Following this, Perseus was used to perform a two-sample Student's t-test between GPS-79 and E35 isolates. A volcano plot was generated with a setting of $S_0 = 1$ and a False Discovery Rate (FDR = 0.05) to determine which proteins were significantly enriched in any experimental group. The shape of the cut-off curve (the volcano) was calculated by Perseus and is described in detail by Rudolph and Cox (2019).

2.8. Bioinformatics analyses

Sequences of proteins whose abundance differed between the aggressive isolate GPS79 and less aggressive E35 isolate were uploaded to SecretomeP v2.0 (http://www.cbs.dtu.dk/services/SecretomeP/) (Bendtsen et al., 2004) in FASTA format. The search was performed using settings for mammals. Ontology annotations were generated using the BLAST2GO tool (Conesa et al., 2005) (www.blast2go.org) by querying with BLASTp against the nonredundant database at NCBI (May 2021). Annotation was based on the NCBI description lines from the BLASTp return with the smallest E-value. Further analyses were performed to predict potential signal-peptide signatures using SignalP (v4.1 and v6.0) (http://www.cbs.dtu.dk/services/Signal P/) with the default settings for eukaryotes (Petersen et al., 2011). Where known secretory signals were identified, proteins were filtered further to eliminate those with a known mitochondrial and chloroplast localization signal, using TargetP (v2.0) (http://www.cbs.dtu.dk/services/TargetP/) (Emanuelsson et al., 2000) using the default settings for plant organisms. Effector candidates among differentiated proteins of both isolates were estimated by effectorP (3.0) (http://effectorp.csiro.au/index.html) (Sperschneider et al., 2018). Classification of protein families was also done using the Interpro database (http://www.ebi.ac.uk/interpro/) (Blum et al., 2021), and lipase domains of identified proteins were predicted from the LED database (https://led.biocatnet.de/sequence-browser) (Fischer and Pleiss, 2003). Subcellular localization prediction was analyzed using the following webtools; Localizer (http://localizer.csiro.au/), WolfPSORT (https://wolfpsort.hgc.jp/) (Sperschneider et al., 2017; Horton et al., 2007). The ClustalW webtool (https://www.ebi.ac.uk/Tools/msa/clustalo/) predicted the similarity using multiple sequence alignment analysis on candidate effectorome dataset (Sievers et al., 2011). The phylogenetic tree was visualized by iTOL web-tool (https://itol.embl.de/) (Letunic and Bork, 2016). Motif discovery analysis on effectorome sets was conducted using MEME motif finder (https://meme-suite.org/meme/tools/meme) (Bailey et al., 2015).

2.9. Cloning and characterizing effector PtmNPP1

The total RNA of barley inoculated with GPS79 was isolated using QIAzol lysis reagent (QIAGEN). After Dnase treatment, cDNA was synthesized using SuperScript IV (Invitrogen). PtmNPP1 was amplified from cDNA by PCR and cloned into pTRBO (pJL48). The pTRBO-PtmNPP1 and pTRBO-PtmNPP1-ΔSP (the latter lacking the signal sequence) vectors were validated by DNA sequencing and used to transform *Agrobacterium tumefaciens* GV3101 by electroporation. *A. tumefaciens* GV3101 mediated gene transfer was conducted as described previously by Ozketen et al. (2020). Briefly, the bacteria

carrying the plasmids were harvested directly from selective agar media after two days of incubation at 28 °C. Two washing steps were performed with sterile water, and twice with gene transfer-induction buffer (10 mM MES, pH 5.6, 10 mM $MgCl_2$). The final cell concentration was adjusted to 0.4 at A_{600nm} for infiltration. pTRBO-GFP was used as the negative control and Inf1 as the positive control. The bacteria were injected into *Nicotiana benthamiana* leaves using a needleless syringe. The results of phenotypic changes were recorded over the next 2–6 days.

2.10. Pride

The mass spectrometry proteomics data have been deposited to the ProteomeXchange Consortium via the PRIDE partner repository with the dataset identifier PXD035240.

3. Results

3.1. Ptm E35 was less aggressive than Ptm GPS79 on barley cultivar Bülbül 89

The following disease ratings were determined for the two *Ptm* isolates used. *Ptm* E35 showed an average rating of 3 (moderately resistant) on barley leaves and GPS79 an average rating of 7 (moderately susceptible), when inoculated on the susceptible barley cultivar Bülbül 89 using the Tekauz disease scale (Tekauz, 1985) (Fig. 1). In this scale, the classes for *Ptm* were defined as follows: 1 = resistant (R); 2 = R to moderately resistant (MR); 3 = MR; 5 = MR to moderately susceptible (MS); 7 = MS; 8 = MS to susceptible (S); and 9 = S.

3.2. The Ptm secretome of GPS79 was richer than that of E35

The medium of collected secretome contains host (barley) leaves to induce secretion by mimicking the real nature of the pathogen. The average yield of secreted proteins from the more aggressive GPS79 isolate was slightly higher than that of E35. On average, from four biological replicates, GPS79 yielded 39.03 mg/mL proteins whereas E35 yielded 31.12 mg/mL. In total, the LC-MS analyses identified 1175 proteins after the removal of potential contaminants and decoys. Of these, 931 were from *Ptm* and the rest (244) from *H. vulgare*, which was present as leaf sections in the medium. After removing proteins that did not occur in at least three biological replicates, 478 proteins remained for analysis. These are shown on a volcano plot (Fig. 2) where proteins falling to the left of the volcano are more abundant in GPS79 relative to E35, and vice-versa. All 160 proteins falling outside of the volcano (colored in red) differed significantly in abundance by at least 2-fold between GPS79 and E35. These 160 proteins are shown in Tables S2A and S2B and their Interpro classifications are summarized in Table 1. All the proteins from the two isolates were divided into 59 protein families. In GPS79 and E35, 66 and 20 proteins were lacking a predicted family, respectively. Proteins belonging to the aspartic peptidase A1 family, peptidase M13, uncharacterized protein family UPF0311, and multicopper oxidase family were common to both isolates. Glycoside hydrolase family proteins, except glycoside hydrolase family 61 in E35, were expressed more abundantly in the more aggressive isolate, GPS79. The more aggressive isolate GPS79 appears to secrete more abundant CWDEs and Cazymes in the growth medium containing host leaves. Ten peptidase families were observed with only two appearing in both isolates. The proteins inside the volcano (318 of them) did not differ significantly in abundance between the two isolates.

The results of the BLAST-2-GO analysis distribution are given in Fig. 3. In this figure, annotations are classified into 11 groups, secreted proteins from GPS79 are represented in all classes but there are no proteins from localization, biological regulation, response to stimulus, reproductive process, and multi-organism process localization for the E35 isolate. The combined graph of Annotation Distribution is given in Fig. 3.

Fig. 1. Reactions of the *Pyrenophora teres* f. *maculata* isolates E35 (A) and GPS79 (B) seven days after inoculation on the leaves of the susceptible barley cultivar Bülbül 89.

In silico predictions of protein domains yielded nine proteins predicted to have a carbohydrate-active enzymatic region for E35 and 55 for GPS79. One of these proteins from E35 was uncharacterized, however, all proteins with Cazy domains in GPS79 had known homologs. In E35 four of the differentially abundant secreted proteins had a lipase domain, compared to 27 proteins in GPS79 (Table S3).

The functional groups of carbohydrate-active regions of proteins from the E35 isolate had carbohydrate esterase and glycosyl transferase activities. Carbohydrate-binding modules and auxiliary activities functions were dominant. In the GPS79 secretome 37 proteins contained glycoside hydrolase domains, 12 had auxiliary activity domains and four proteins contained a carbohydrate esterase domain. In GPS79 no glycosyl transferases and carbohydrate-binding module were seen, instead, glucoside hydrolase activities dominated (37 of 53 Cazyme).

3.3. In silico effectorome prediction revealed a set of candidate proteins

Proteome profiling of both E35 and GPS79 isolates revealed that 1175 proteins were found in the barley-induced secretome; 936 of these were returned from *Ptm*, the remainder (239) from barley. The repertoire of secreted proteins is crucial to phytopathogenic fungi since the interaction with the host depends on them (Bahram and Netherway,

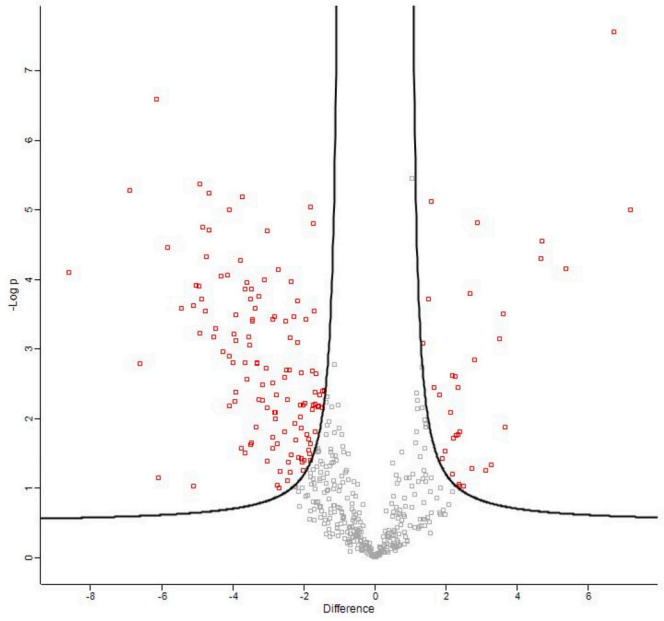

Fig. 2. Volcano Plot of the secretome profiles of *Pyrenophora teres* f. *maculata* isolates E35 and GPS79 seven days after inoculation on the leaves of the susceptible barley cultivar Bülbül 89.

2021). We scrutinized the secreted proteins using *in silico* analyses with the pipeline described in Fig. 4. Of the 382 proteins bearing a putative signal peptide sequence in their N terminus, 135 of them were predicted to be cytoplasmic or apoplastic effectors by the Effector 3.0 algorithm (Table S3L). The predicted effectorome set of GPS79 was larger than E35 as in the secretome data above. The comparison of the two secretomes is presented graphically in Fig. 5A. As we analyzed the percentages of predicted effectorome and secretome sets scrutinized from E35, GPS79, or reference *Ptm* (FGOB10Ptm-1) proteome data, we have pinpointed 49.7% of the E35 and 42.4% of the GPS79 predicted as secretome whereas only 8.0% of the *Ptm* are listed as secretome as the pipeline with same parameters applied. Correspondently, 17.0% and 15.1% of the proteins from E35 and GPS79 sets listed as predicted effectorome exceeding the 3.2% of the proteins from *Ptm* data.

The multiple clustal alignments among all predicted effectorome sets of GPS79 and E35 showed that there were four main clades in the phylogenetic tree given in Fig. 5B. We scanned the effectorome dataset to detect any conserved motifs using the MEME motif finder tool. Detecting conserved protein motifs among protein sequences is an efficient strategy to classify and discover functions such as host translocation motifs etc (Saunders et al., 2012). We observed a 'CCS[QL][YS] GYCGT' motif present in 11 of 135 (~8%) effector candidates. Furthermore, we detected 73 occurrences of 'Y/F/WXC' in the full-length protein sequences without N-terminal signal peptide. This motif has been reported as conserved in the N-terminus of the effectors of the powdery mildews and rusts (Godfrey et al., 2010). The detected motifs were at N or C termini without specific clustering to either end of the protein sequences. The 'Y/F/WXC' motif is overpresented in the predicted secretome and effectorome sets of our identified protein list compared to whole protein, secretome, and effectorome sets of *Ptm*. 387 motifs were detected on the predicted *Ptm* secretome (48.7%) while 229 motifs are present in the predicted secretome of our protein set (57.1%). In parallel with this finding, 159 motifs were detected on the predicted *Ptm* effectorome (50.3%) as 73 motifs occur in the predicted effectorome of our protein set (54.1%). Other common motifs such as [LI]xAR or RXLR were not present abundantly, however, the domain annotations indicated two candidates bearing a LysM domain (PTMSG1_04324 and PTMSG1_10188), one candidate (PTMSG1_02779) had a CFEM domain

Table 1
List of protein families/superfamilies in the secretome of *Ptm* isolates.

Family/Superfamily	IPR No	CAZy	Isolate Name
Aldose 1-/Glucose-6-phosphate 1-epimerase	IPR008183	_	GPS79
Glucose-methanol-choline oxidoreductase	IPR036188	_	GPS79
Fungal antigen PRA1-like	IPR039124	_	GPS79
Catalase, mono-functional, heme-containing	IPR018028	_	GPS79
Glycoside hydrolase family 1	IPR001360	AA3_2 (36–617)	GPS79
Glycoside hydrolase family 10	IPR044846	GH10 (116–409)	GPS79
Glycoside hydrolase family 12	IPR002594	GH12 (97–243)	GPS79
Glycoside hydrolase, family 16, CRH1, predicted	IPR017168	GH16_18 (67–222)	GPS79
Glycoside hydrolase family 17	IPR000490	GH17 (25–305)	GPS79
Glycoside hydrolase family 31	IPR000322	GH31 (260–788)	GPS79
Glycoside hydrolase, family 32	IPR001362	GH32 (56–412)	GPS79
Glycoside hydrolase family 36	IPR002252	GH36 (33–723)	GPS79
Glycoside hydrolase, family 43	IPR006710	GH43_26 (32–352)	GPS79
Glycoside hydrolase family 47	IPR001382	GH47 (45–504)	GPS79
Glycoside hydrolase, family 61	IPR005103	AA9(6–229)	E35
Glycoside hydrolase, family 62, arabinosidase	IPR005193	GH62 (27–300)	GPS79
Glycoside hydrolase family 76	IPR005198	GH76 (30–404)	GPS79
Aspartic peptidase A1 family	IPR001461	_	GPS79, E35, E35-HORVU
Peptidase S51	IPR005320	_	GPS79
Peptidase M13	IPR000718	_	GPS79, E35
Uncharacterized protein family UPF0311	IPR020915	_	GPS79, E35
Esterase, PHB depolymerase	IPR010126	CE1 (43–241)	GPS79
Glucosamine 6-phosphate N-acetyltransferase	IPR039143	_	GPS79
Protein of unknown function DUF1993	IPR018531	_	GPS79
Succinylglutamate desuccinylase/ aspartoacylase	IPR007036	_	GPS79
Peptidase S10, serine carboxypeptidase	IPR001563	_	GPS79
Pyridoxal phosphate-dependent decarboxylase	IPR002129	_	GPS79
YjgF/YER057c/UK114 family	IPR006175	_	GPS79
Kre9/Knh1 family	IPR018466	_	GPS79
Peptidase S28	IPR008758	_	GPS79
Glucose-methanol-choline oxidoreductase	IPR012132	AA3_2 (52–630)	GPS79
Peptidase S1A, chymotrypsin family	IPR001314	_	GPS79
Peptidase M28, SGAP-like	IPR041756	_	GPS79
Gamma-glutamyltranspeptidase	IPR000101	_	GPS79
Peptidase S8, subtilisin-related	IPR015500	_	GPS79
Exo-beta-D-glucosaminidase/ Endo-beta-mannosidase	IPR043534	GH2 (52–707)	GPS79
Alpha-1,2-mannosidase, putative	IPR005887	GH92 (270–779)	GPS79
Glucanosyltransferase	IPR004886	GH72 (29–330)	GPS79
2-amino-3-carboxymuconate-6-semialdehyde decarboxylase	IPR032465	_	GPS79
YtcJ like	IPR033932	_	GPS79
Glutamate/phenylalanine/ leucine/valine dehydrogenase	IPR006095	_	GPS79
Cobalamin-independent methionine synthase	IPR006276	_	GPS79
Aminopeptidase Y	IPR029514	_	GPS79

(*continued on next page*)

Table 1 (*continued*)

Family/Superfamily	IPR No	CAZy	Isolate Name
Alkaline Phosphatase	IPR001952	_	GPS79
Histidine phosphatase superfamily, clade-2	IPR000560	_	GPS79
Lactonase, 7-bladed beta propeller	IPR019405	_	GPS79
Beta-hexosaminidase	IPR025705	GH20 (187–557)	GPS79
Ribonuclease T2, eukaryotic	IPR001568	_	GPS79
Multicopper Oxidase	IPR045087	AA1_3 (62–376)	GPS79, E35
Tannase/feruloyl esterase	IPR011118		GPS79
Deoxyribonuclease NucA/NucB	IPR029476	_	E35
Heme-binding peroxidase Ccp1-like	IPR044831	AA2 (68–211)	E35
Cutinase/acetylxylan esterase	IPR000675	CE5 (36–243)	E35
Alpha-hydroxy acid dehydrogenase, FMN-dependent	IPR012133	_	E35
Blue (type 1) copper protein, plastocyanin-type	IPR001235	_	E35-HORVU
Plant Peroxidase	IPR000823	AA2 (55–318)	GPS79-HORVU
Triosephosphate isomerase	IPR000652	_	E35-HORVU

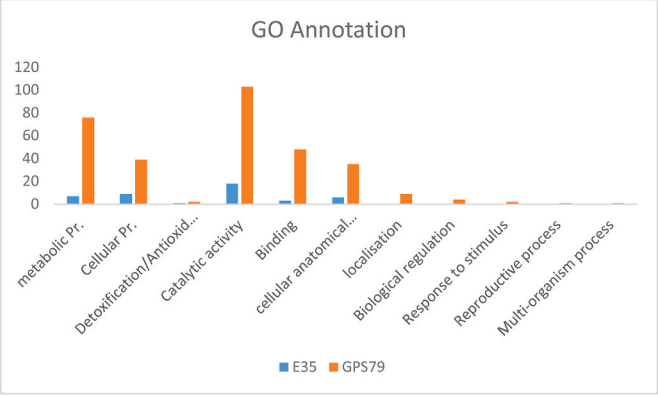

Fig. 3. Annotation distribution of differentiated proteins among *Pyrenophora teres* f. *maculata* isolates E35 and GPS79. Annotation analysis was performed by Blast2GO (www.blast2go.org).

motif (cysteine enriched cell death elicitor domain) and an NPP1 domain motif was present in a candidate effector (PTMSG1_04452). The LysM domain and CFEM domain motifs were also indicated as effector candidates by Ismail and Able (2016).

The majority of the candidate effectors showed no homology to known proteins and were unannotated as expected. In addition, the candidate effectors were small in size (<300 amino acids in length); had a high cysteine content; and possessed a known secretion signal (Sperschneider et al., 2018). For GPS79, two candidate effectors had five cysteine residues (GPS42-PTMSG1_04052 and GPS101-PTMSG1_08532), three of them had four (GPS43-PTMSG1_04069, GPS72-PTMSG1_08912, PTMSG1_06179) and one of them had seven residues (GPS67-PTMSG1_06179). One candidate (GPS38-PTMSG1_03757) had no cysteine but was predicted based on size (184 amino acids in length) and unknown function. For E35, secreted effector candidates were PTMSG1_03007, PTMSG1_05839, PTMSG 1_06793, and PTMSG1_09377. Among these PTMSG1_05839 and PTMSG1_03007 were remarkable with their very short aa length (120 and 130 aa) and high cysteine content (eight and seven residues, respectively). All predicted effector candidates were apoplastic and cytoplasmic effectors.

3.4. *PtmNPP1 caused cell death symptoms on N. benthamiana*

Experimental validation for a candidate effector from the list

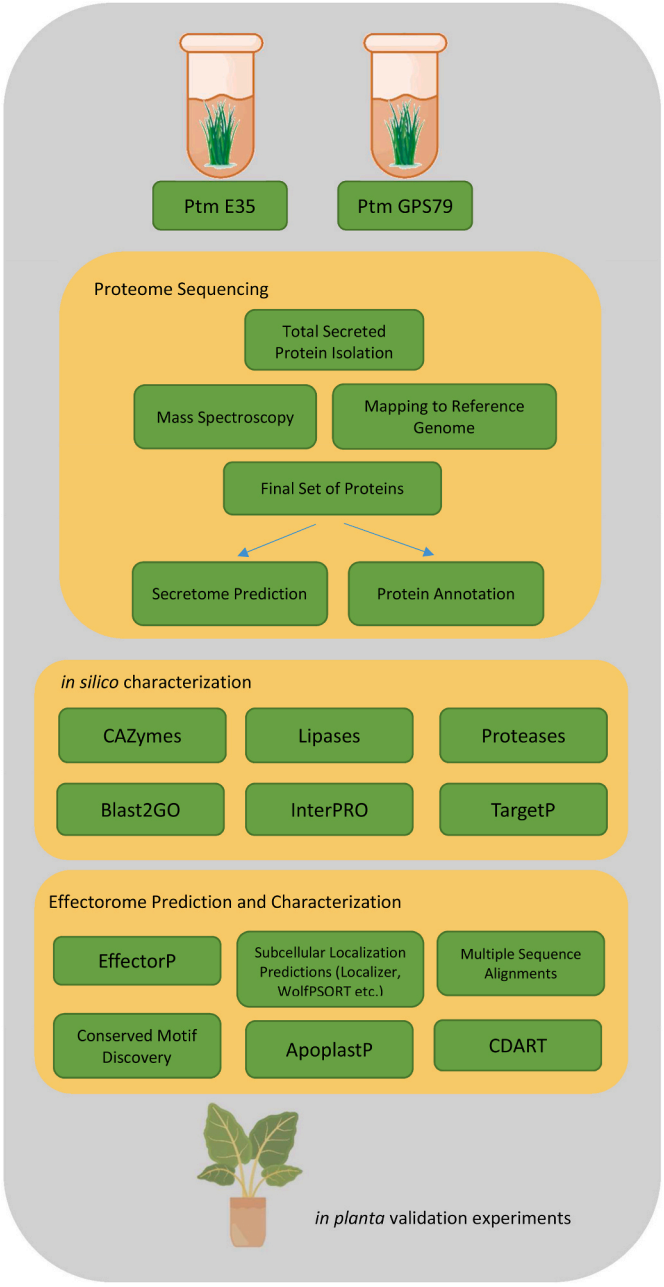

Fig. 4. Comparative Ptm secretome data Mining pipeline.

(Table S3L) was conducted to provide evidence for the accuracy of *in silico* analysis. To date no effector proteins of *Ptm* have been reported, hence we selected an effector candidate (PTMSG1_04452) expected to have detectable phenotypic symptoms in planta. The cell death inducers or elicitors are a crucial class of effectors. The plant-pathogen interaction depends on these types of molecular recognition mechanisms. The observed cell death may be advantageous to the pathogen for example to trigger necrosis or to the host to halt or slow down the infection. Necrosis-inducing proteins (NPPs) are well-studied effectors reported for *Phytophthora* and other plant fungal pathogens (Fellbrich et al., 2002; Bailey, 1995; Nelson et al., 1997). We have shown that PTMSG1_04452 (PtmNPP1) containing a NPP1 domain is expressed in GPS79, and we hypothesized that this protein should trigger cell death upon expression *in planta*.

We observed cell death induced by both *Ptm*NPP1 and *Ptm*NPP1-ΔSP (the latter lacking the N-terminal secretion signal). However, in *Ptm*NPP1-ΔSP cell death was delayed (Fig. 6). Previous studies by our

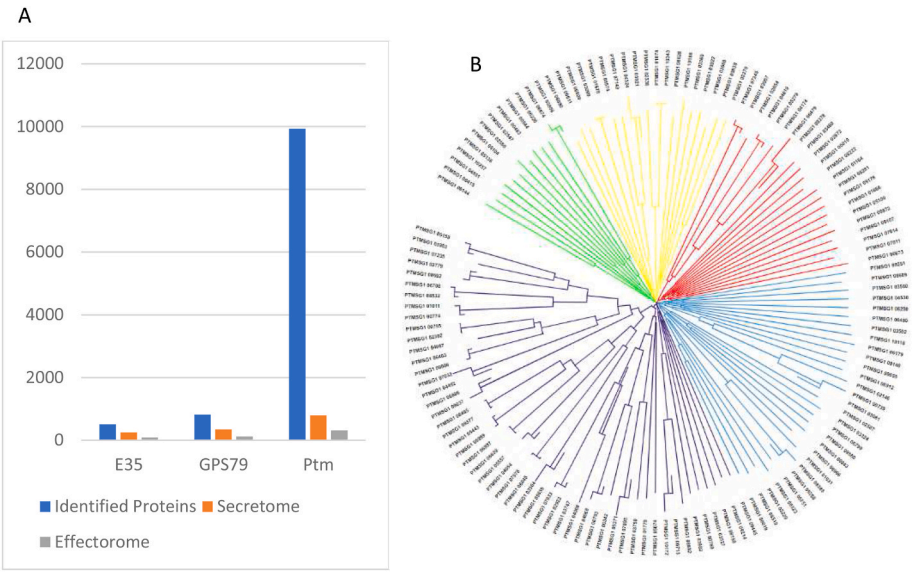

Fig. 5. *in silico* prediction and characterization analysis of *Ptm* effectorome. A) The comparison of the number of predicted proteins between GPS79, E35, and predicted *Ptm* Proteome B) phylogenetic analysis on candidate effectorome data. Each color represents major related groups in terms of multiple sequence alignments. (For interpretation of the references to color in this figure legend, the reader is referred to the Web version of this article.)

group indicated that retaining the signal peptide is important for apoplastic effectors function (e.g., PstSCR1), but not for cytoplasmic or organelle targeting effectors, like the chloroplast targeting/cell death suppressor PSTG_10917 (Dagvadorj et al., 2017; Ozketen et al., 2020). We predicted *Ptm* NPP1 to be an apoplastic effector, i.e. the signal peptide could be dispensed with for effector function. The observed delay in cell death on plant leaves suggests that PtmNPP1 may need to be secreted into the apoplast to induce cell death in a swift manner, but a slower trigger of defense response occurs without a secretion signal.

4. Discussion

Obtaining a secretome *in vitro* is relatively easy with *Ptm* as it grows well in PDB. Initial studies indicated that the secretome is complex (unpublished observation), and likely more physiologically relevant if host tissue was present in the PDB; this was achieved by adding leaf segments to the media. This was also reported for *F. graminearum* (Rampitsch et al., 2013) where amendment of the growth medium with host tissue increased the secretome complexity, presumably by providing host factors into the medium which helped initiate pathogenesis and established a pathogenesis-ready secretome.

A total of 244 proteins were returned from the barley genomic database (Table S1). These were present in at least one replicate and were largely metabolic enzymes (e.g., Ribulose Bisphosphate Carboxylase) that had likely leaked out of damaged leaf tissue. However, at least nine peroxidases, two chitinases, and some other defense-related proteins were also detected. It is unclear whether these were produced in response to *Ptm*, or as a general wounding response of the detached leaf. It is likely that these proteins, along with other non-proteinaceous host molecules, contributed to the richness of the *Ptm* secretomes. Chitinase, peroxidases, germin-like proteins, and thioredoxin-dependent peroxiredoxin were identified as host proteins in the media of the aggressive isolate GPS79, whereas triose phosphate isomerase, plastocyanin, starch synthase, chloroplastic/amyloplastic were abundant in media containing the less aggressive isolate E35. In general, chitinase, germinlike proteins and peroxidases are induced against biotrophic

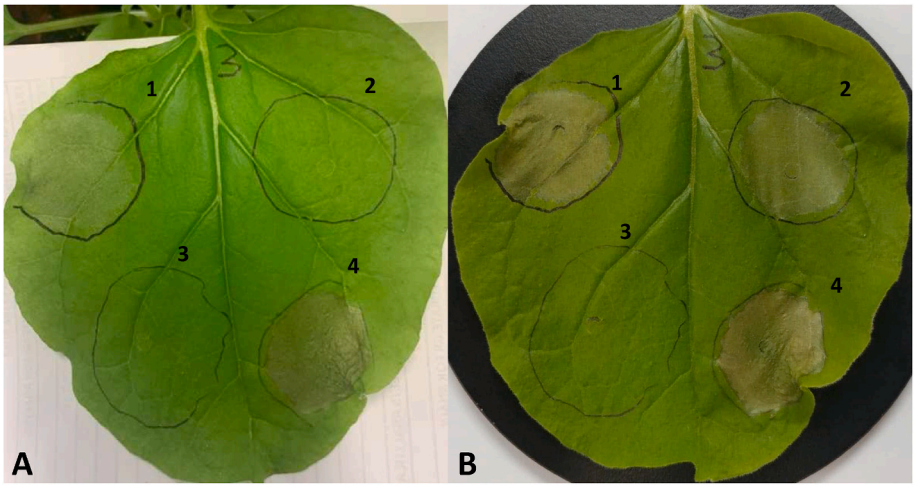

Fig. 6. Both *Ptm*NPP1 or *Ptm*NPP1-ΔSP are able to induce cell death on *Nicotiana benthamiana* leaves. 1-*Ptm*NPP1 (upper left ring), 2-*Ptm*NPP1-ΔSP (upper right), 3-GFP (lower left) and 4-Inf1 (Lower right). **A)** 3rd day and **B)** 5th-day photos of the same leaf sample. GFP: Green Fluorescent protein as negative control, Inf1: cell death elicitor as positive control. (For interpretation of the references to color in this figure legend, the reader is referred to the Web version of this article.)

pathogens to improve plant resistance, for example, chitinase was observed during the resistance against powdery mildew infection in wheat (Oldach et al., 2001). In response to the infection of *M. truncatula* by the hemibiotrophic pathogen *C. trifolii* expression of pathogenesis-related proteins such as chitinase and peroxidases was exhibited in a time-dependent manner (Torregrosa et al., 2004). Expressions of these pathogenesis-related proteins were not sustained along the infection process (Métraux et al., 2009).

The likeliest candidate proteins with important roles in modulating the aggressiveness phenotype can be broadly broken down into cell wall degrading enzymes (CWDEs); proteolytic enzymes; oxidoreductases; and other pathogenesis-related proteins not covered by these groups.

4.1. There are large differences in cell wall degrading enzymes between the GPS79 and E35 secretomes

The importance of cell wall degrading enzymes (CWDEs) for plant pathogens is well known (Kubicek et al., 2014). It was therefore encouraging to find 17 CWDEs increased in abundance in the aggressive GPS79 isolate and only one in the less aggressive E35 isolate. These were identified as glycoside hydrolase (GH) family members by InterPro. Querying the CAZy database yielded 38 GH family members returned for GPS79 and none for E35, indicating that the ability to degrade host cell wall components is an important determinant of aggressiveness in SFNB, as has indeed been shown for many other plant pathogens, e.g., *Phaeosphaeria nodorum* (Lalaoui et al., 2000).

There are several subgroups of glycoside hydrolases. GH3, GH12, and GH 16 degrade beta-glucan, cellulose, and hemicellulose respectively (Zhao et al., 2014) and these were all identified in the GPS79 secretome. GH12 is a known virulence factor and a pathogen-associated molecular pattern (PAMP) in the *Phytophthora sojae*-soybean interaction where it can trigger defense responses including cell death (Ma et al., 2015). In addition, two members of the GH family act as an inducer of plant immunity in the soilborne fungal plant pathogen, *Verticillium dahliae* (Gui et al., 2017). Furthermore, GH12 was shown to degrade the cell wall to introduce effector molecules during the *Setosphaeria turcica*-maize interaction (Meng et al., 2022). GH12 members were also observed in the interaction between *P. tritici-repentis* and wheat (Manning et al., 2013) and *Ptt*-barley in Australian lines (Ismail and Able, 2016).

The GH16 family is present in the predicted proteomes of 94 representative fungi (Zhao et al., 2014). We identified one protein belonging to this family with similarity to Crh1 according to Interpro, and two proteins were returned from the CAZy database. GH16 proteins are crucial for appressoria formation in the rice blast pathogen *Magnaporthe oryzae* (Franck et al., 2013) and more importantly also in an aggressive Australian isolate of *Ptt* (Ismail and Able, 2016).

GH7, 10, and 43 belong to the xylanase group in the CAZy database; these enzymes cleave the β-1,4-glucosidic bonds in cellulose, although some GH7 members also act on xylan (Rafiei et al., 2021); GH7 was identified in the GPS79 isolate. This GH family was described in the interaction between *P. tritici-repentis*-wheat (Manning et al., 2013) and in the secretome of *Ptt* in Australian lines (Ismail and Able, 2016). GH7 is involved in virulence or the elicitation of plant immunity, (Van Vu et al., 2012). When GH7 and 10 were silenced in *M. oryzae* the aggressiveness of the pathogen was decreased, with GH10 showing a greater effect (Nguyen et al., 2011).

GH76 family proteins, defined as containing an α-1,6-mannanase domain, were identified in GPS79. The function of some of these family members was elucidated in the phytopathogen *Pyricularia oryzae*. It was found that lack of this protein causes a reduction in colony growth by approximately 3-fold and a 50-fold attenuation in conidiation. GH76 members affect appressorium maturation and thus cause attenuated penetration, and lack of GH76 decreased *P. oryzae* aggressiveness (Pan et al., 2021). This is the first report of this protein in *Ptm* and it was not observed in the secretome of *Ptt (Ismail and Able, 2016)*.

GH61 was identified in E35, the isolate with low aggressiveness. The GH61 family hydrolyzes the cell wall lignocellulosic structure (Harris et al., 2010).

The present study identified 37 proteins belonging to 26 different GH families in GPS79 when the CAZy database was queried by BLASTp, and 17 classes were identified using the Interpro classification. GH1, GH19, GH36, GH51, GH55, GH65, GH72, GH76, GH92, GH93, and GH131 have not previously been reported in *Pyrenophora* spp. secretome or proteome studies. (Suppl Table 2). In addition to these glycohydrolase family proteins, one further cell wall-related protein, belonging to the Kre9/Knh1 family, was more abundant in GPS79. Reports of the function of this protein family are from *Cryptococcus neoformans* and *Candida albicans* (Dijkgraaf et al., 1996; Gilbert et al., 2010). Kre9/Knh1 protein family has involved in the synthesis of β-1,6 glucan from cell wall polysaccharides. This polysaccharide interacts with both glycoproteins and other cell wall components and Gilbert et al.*(2010)* showed that when the fungus has mutations in some members of this family, cell wall synthesis decreased remarkably, and the growth rate was slow. Kre9/Knh1 protein family was identified as a candidate effector in *Puccinia triticina* pathotypes THTT and THTS (Wei et al., 2020).

Some GH family proteins are modulated by carbon and nitrogen availability, especially when one or both of these nutrients becomes limiting. Thus, GH28, GH32, and GH43 were increased in abundance in nitrogen deficient *Eucalyptus* infected with the foliar pathogen *Teratosphaeria destructans* (Havenga et al., 2021) and also in the *Ptt* secretome *in vitro* described here. On the other hand, GH16 and GH 131 family proteins were shown to be decreased in abundance in the *Eucalyptus/T. destructans* interaction, however, these proteins were increased in our *Ptm* secretomes *in vitro*. In *Magnaporthe oryzae* grown under limited nitrogen *in vitro*, Oh and colleagues (2020) reported more than 500 proteins responding to this stress, and moreover were able to infer a link between nitrogen starvation pathogenicity in *M. oryzae*. *Aspergillus niger* grown under carbon-limiting conditions showed increased levels of GH18 and GH20 abundance (Nitsche et al., 2012); homologs of these proteins, (PTMSG1_08592, PTMSG1_09172) were also increased in the GPS79 secretome *in vitro*.

4.2. Peptidases are more highly represented in the GPS79 secretome

Peptidases are another important group of enzymes likely to have important roles in determining aggressiveness phenotypes. Although these enzymes have important housekeeping roles, they are also deployed during the plant-pathogen interaction where they serve to break down each other's defenses and effectors, many of which are proteins or peptides. This has been extensively reviewed, recently by Figueiredo et al. (2021). In the aggressive isolate GPS79 secretome, several peptidases were seen exclusively – these were a family of peptidase S8, peptidase S10, peptidase S28, peptidase S1A, and peptidase S51 and peptidase M28, aminopeptidase Y, γ-glutamyl transpeptidase. These classes of peptidases were identified in the tangerine pathotype of *Alternaria alternata* (Fu et al., 2020). In this study peptidases were associated with infection facilitation to get nutrients from the host, although the subtilisin-like proteases had the most prominent role; subtilisin-like proteases were also identified exclusively in the GPS79 secretome. Peptidase S41 is a trypsin-like enzyme, and these have been proposed as general markers of pathogenicity (Dubovenko et al., 2010). Furthermore, peptidases S41 and A1 have been identified in *Ptt*, and it was proposed that these peptidases are responsible for conidial germination and hyphal growth – biological processes necessary to complete the fungal lifecycle which could also affect aggressiveness. Peptidase M13 was not observed in the *Ptt* secretome described by Ismail and Able (2016). The role of this peptidase in plant-pathogenic fungi is unclear, although it is frequently reported in plant-pathogen interactions.

Only the aspartic peptidase A1 family and peptidase M13 were expressed in the secretomes of both isolates. This suggests that peptidases play important roles in aggressiveness. Also, Dikilitas et al. (2018)

compared 5 *Ptm* isolates and 4 *Ptt* isolates differing in virulence for protease activity and glucose production. Virulent *Ptm* isolates produced significantly more protease than the less virulent isolates.

4.3. Oxidoreductases were present in both secretomes

Several proteins with oxidoreductase activity were identified in the secretomes of both *Ptm* isolates. According to the Interpro database, their classes are glucose-methanol-choline oxidoreductases, glu/phe/leu/val dehydrogenase, FMN-dependent α-hydroxy acid dehydrogenase, heme-binding peroxidase Ccp1-like, and multicopper oxidase. The first two were found in GPS79, the second two only in E35. The multicopper oxidase family protein was present in both isolates. Since oxidoreductases were not biased to one secretome in this study, it is difficult to assign a role in aggressiveness to the entire class of oxidoreductases.

The multicopper oxidase family contains ceruloplasmins, ascorbate oxidases, laccases, and nitrite reductases (Kilaru et al., 2006). In our study, laccase-1 and laccase were identified in E35, and multicopper oxidase is identified in GPS79. This class of proteins is crucial for fungi to supply metal from the host to break the host defense mechanism. Liu and colleagues have shown that laccases are required for lignin degradation in the *Setosphaeria turcica*-maize interaction (Liu et al., 2018). Furthermore, they may be required for pathogenicity by melanization of the appressoria, which is required for host penetration, as described in the cucumber anthracnose (Lin et al., 2012). Some proteins of this class were observed in nitrogen-limited *M. oryzae* cultured *in vitro* (Oh et al., 2017) and in the *Eucalyptus/T. destructans* pathosystem (Havenga et al., 2021). These included multicopper oxidase, FAD binding domain proteins, and glucose-methanol-choline oxidoreductase, which were also supported by our results.

In the E35 isolate, we found four proteins increased in abundance that were identified as tyrosinase or tyrosine central domain-containing proteins, (Interpro classification). These are responsible for tyrosine oxidation to produce melanin, which is a protectant for mycelia and spores against several abiotic factors such as dehydration, oxygen, and UV light. Tyrosinase was shown to be crucial for host invasion and appressorium formation of *M. grisea* (Talbot, 2003), and in host cell penetration by *Verticillium dahlia* (El-Bebany et al., 2010). Havenga et al. (2021) and Oh et al. (2017) also reported that several proteins related to melanin biosynthesis were targeted during nitrogen starvation.

Phosphorylcholine phosphatase belongs to the subfamily of the HAD superfamily. It is known that phosphorylcholine phosphatases from bacterial pathogens have played roles in breaking down the host cell membrane. Phylogenetic analysis suggests that it is characteristic of necrotrophic and hemibiotrophic pathogens and has undergone a shared selection process with bacterial plant pathogens (Domenech et al., 2011; Marchler-Bauer et al., 2011). Phosphorylcholine phosphatase has increased in several necrotrophic fungi including *Ptt* (Ismail and Able, 2016; Ismail and Able, 2017), *F. graminearum,* and *Stagonospora nodorum* (Sperschneider et al., 2013). Ismail and Able (2017) proposed that this protein suppresses plant defense response.

4.4. Other virulence, pathogenesis, and morphogenesis-related proteins are associated with aggressiveness

Some pathogenesis-related proteins such as CWDEs and peptidases have already been discussed. Here we focus on proteins with potential roles in pathogenesis and morphology. From these classes of more loosely defined proteins, 23 were more abundant in the GPS79 secretome, and eight in the E35 secretome. Some of these proteins were predicted effector candidates, based on effectorP (Sperschneider et al., 2018), discussed in Section 4.5. Two proteins in this group, with known roles in pathogenicity but no demonstrated role in aggressiveness were aldose 1-epimerase and Ribonuclease T2. The former inter-converts aldose sugars and has been identified in *F. graminearum*-infected wheat (Paper et al., 2007), and also in the *Phytophthora infestans* secretome during interaction with their hosts in the initial biotrophic stages (Raffaele et al., 2010). Furthermore, its abundance was shown to be increased in *Ptt* when it transitions from the biotrophic to the necrotrophic stage in barley (Ismail and Able, 2017), but this protein was not involved in the effector list of Ismail and Able (2016). Effectors with RNase activity, such as RNase T2, have been identified in several fungal pathogens with different lifestyles such as *F. graminearum* (Yang et al., 2021), and *Zymoseptoria tritici* (Kettles et al., 2018) also effectors having ribonuclease folding in biotrophic fungus *Blumeria graminis* (Pennington et al., 2019). This enzyme generally acts by inhibiting host protein synthesis. Guanine-specific ribonuclease N1/T1 and ribonuclease T2 were identified in *Ptt* (*Ismail and Able, 2016*).

4.5. In silico effectorome prediction revealed a set of candidate effector proteins in the secretome

Many small molecules, such as cell wall fragments, small RNAs, and toxins can act as effectors (Toruño et al., 2016) and in fact, the first effectors described in *Ptt* were N-(2-amino-2-carboxyethyl)-aspartic acid, anhydro-aspergillomarasmine A, aspergillomarasmine A and aspergillomarasmine B toxins, which are responsible for causing the chlorotic and necrotic symptoms of NFNB (Smedegård-Petersen, 1977; Bach et al., 1979; Friis et al., 1991; Sarpeleh et al., 2007). The repertoire of secreted proteins is crucial to phytopathogenic fungi since the outcome of the host-pathogen interaction depends on their function (Bahram and Netherway, 2022). Identifying candidate effector proteins in the secretomes presented here, especially amongst the proteins of unknown function, is impeded by a lack of knowledge about these, especially in *Ptt* and *Ptm* (Wyatt and Friesen, 2021). No effector proteins have been confirmed in either to date, although Ismail et al. (2014) have described some strong candidates in *Ptt*. These are PttXyn11A, PttCHFP1, and PttSP1. Candidate effectors for *Ptt* and *Ptm* have recently been reviewed by Clare et al. (2020).

One of the predicted *Ptm* effector candidates was found to contain an NPP1 domain. Proteins with this domain are known effectors in other pathosystems, for example, a 24-kD necrosis and ethylene inducing protein (NEP1) of *Fusarium oxysporum* has been reported to induce cell death in plants (Bailey, 1995; Nelson et al., 1997), and other NEP-like proteins (NLPs) have been described in phytopathogens elsewhere (Pemberton and Salmond, 2004), including the necrosis-inducing *Phytophthora* protein 1 (NPP1) (Fellbrich et al., 2002). Although *Ptm*NPP1, was observed in only one replicate of GPS79, we reasoned that since we could clone *Ptm*NPP1 from GPS79 mRNA, *Ptm*NPP1 was present in the GPS79 secretome.

In hemibiotrophic fungal pathogens formation of haustoria or haustoria-like vesicles, generally signals the transition from a biotrophic to the necrotrophic phase. Within this class of pathogens *M. oryzae* and *Puccinia* spp. have been studied intensively and, in general, their effectors target the cytoplasm or apoplastic fluid of the host. In *P. triticina*, there is a dramatic increase of candidate-secreted effector proteins after haustoria have formed (Rampitsch et al., 2019). In *M. oryzae* effectors are secreted from the biotrophic interface complex (BIC) and are targeted to the host cytoplasm. Secreted effectors from appressoria are targeted to the apoplast of the host (Giraldo et al., 2013; Zhang and Xu, 2014). It is not known whether this is also the case in *Ptm*, and indeed an *in vitro*-based secretome is unlikely to yield an exhaustive effectorome.

5. Conclusion

The secretome of plant pathogens is a rich source of proteins with important roles in aggressiveness and virulence. Hosts can detect pathogens early on when they recognize pathogen-associated molecular patterns, which can either be pathogen-secreted proteins themselves or the degradation products of pathogen-secreted lytic enzymes – for example, carbohydrate fragments resulting from degraded cell walls. It is therefore important to build up an inventory of secretomes, especially

from aggressive isolates. Here we have used a strategy that permits deep proteome coverage of the secretomes of two *Ptm* isolates, and we have demonstrated that there are important differences in their lytic enzyme contents, which appear to be responsible for their aggressiveness phenotypes.

CRediT authorship contribution statement

Mahmut Emir: Validation, Investigation. **Ahmet Caglar Ozketen:** Validation, Investigation, Data curation, Methodology, Writing – review & editing. **Ayse Andac Ozketen:** Validation, Investigation. **Arzu Çelik Oğuz:** Validation, Investigation. **Mei Huang:** Validation, Investigation, Data curation. **Aziz Karakaya:** Validation, Investigation, Methodology, Writing – review & editing. **Christof Rampitsch:** Validation, Investigation, Data curation, Methodology, Writing – review & editing. **Aslihan Gunel:** Conceptualization, Methodology, Investigation, Validation, Funding acquisition, Supervision, Writing – review & editing.

Declaration of competing interest

The authors declare the following financial interests/personal relationships which may be considered as potential competing interests: Aslihan Gunel reports financial support was provided by The Scientific and Technological Research Council of Turkey.

Data availability

We uploaded supplementary data. In addition, we shared the Pride repository username and password with the editor for reviewers.

Acknowledgements

The authors thank Nathan Wyatt for guiding us to the latest *Pyrenophora teres* f. *maculata* genome. This work was funded by a grant from TUBITAK to A.G with 114Z084 project number and to Kirsehir Ahi Evran University for its infrastructure support with PYO-FEN.4001.16.002 and FEF.B2.16.005 projects.

Appendix A. Supplementary data

Supplementary data to this article can be found online at https://doi.org/10.1016/j.jplph.2022.153839.

References

Bach, E., Christensen, S., Dalgaard, L., Larsen, P.O., Olsen, C.E., Smedegård-Petersen, V., 1979. Structures, properties and relationship to the aspergillomarasmines of toxins produced by Pyrenophora teres. Physiol. Plant Pathol. 14 (1), 41–46.

Bahram, M., Netherway, T., 2022. Fungi as mediators linking organisms and ecosystems. FEMS Microbiol. Rev. 46 (2) fuab058.

Bailey, B.A., 1995. Purification of a protein from culture filtrates of *Fusarium oxysporum* that induces ethylene and necrosis in leaves of *Erythroxylum coca*. Phytopathology 85, 1250–1255.

Bailey, T.L., Johnson, J., Grant, C.E., Noble, W.S., 2015. The MEME suite. Nucleic Acids Res. 43 (W1), W39–W49.

Bendtsen, J.D., Jensen, L.J., Blom, N., Von Heijne, G., Brunak, S., 2004. Feature-based prediction of non-classical and leaderless protein secretion. Protein Eng. Des. Sel. 17 (4), 349–356.

Blum, M., Chang, H.Y., Chuguransky, S., Grego, T., Kandasaamy, S., Mitchell, A., Nuka, G., Paysan-Lafosse, T., Qureshi, M., Raj, S., Richardson, L., Salazar, G.A., Williams, L., Bork, P., Bridge, A., Gough, J., Haft, D.H., Letunic, I., Marchler-Bauer, A., Mi, H., Natale, D.A., Necci, M., Orengo, C.A., Pandurangan, A.P., Rivoire, C., Sigrist, C.J.A., Sillitoe, I., Thanki, N., Thomas, P.D., Tosatto, S.C.E., Wu, C.H., Bateman, A., Finn, R.D., 2021. The InterPro protein families and domains database: 20 years on. Nucleic Acids Res. 49 (D1), D344–D354.

Bradshaw, M.J., Bartholomew, H.P., Fonseca, J.M., Gaskins, V.L., Prusky, D., Jurick, W. M., 2021. Delivering the goods: fungal secretion modulates virulence during host-pathogen interactions. Fun. Biol. Rev. 36, 76–86.

Çelik Oğuz, A., Karakaya, A., 2017. Pathotypes of *Pyrenophora teres* on barley in Turkey. Phytopathol. Mediterr. 56 (2), 224–234.

Clare, S.J., Wyatt, N.A., Brueggeman, R.S., Friesen, T.L., 2020. Research advances in the *Pyrenophora teres*-barley interaction. Mol. Plant Pathol. 21 (2), 272–288.

Conesa, A., Götz, S., García-Gómez, J.M., Terol, J., Talón, M., Robles, M., 2005. Blast2GO: a universal tool for annotation, visualization and analysis in functional genomics research. Bioinformatics 21 (18), 3674–3676.

Coval, S.J., Hradil, C.M., Lu, H.S.M., Clardy, J., Satouri, S., Strobel, G.A., 1990. Pyrenoline-A and -B, two new phytotoxins from *Pyrenophora teres*. Tetrahedron Lett. 31 (15), 2117–2120.

Dagvadorj, B., Ozketen, A.C., Andac, A., Duggan, C., Bozkurt, T.O., Akkaya, M.S., 2017. A *Puccinia striiformis* f. *sp. tritici* secreted protein activates plant immunity at the cell surface. Sci. Rep. 7 (1), 1141.

Demirci, Y.E., Inan, C., Günel, A., Maytalman, D., Mert, Z., Baykal, A.T., Korkut, Ş.V., Arda, N., Hasançebi, S., 2016. Proteome profiling of the compatible interaction between wheat and stripe rust. Eur. J. Plant Pathol. 145 (4), 941–962.

Dijkgraaf, G.J., Brown, J.L., Bussey, H., 1996. The KNH1 gene of *Saccharomyces cerevisiae* is a functional homolog of KRE9. Yeast 12 (7), 683–692.

Dikilitas, M., Çelik Oğuz, A., Karakaya, A., 2018. Extracellular protease activity and glucose production in isolates of net blotch pathogens differing in virulence. Zemdirbyste-Agric. 105 (1), 89–94.

Domenech, C.E., Otero, L.H., Beassoni, P.R., Lisa, A.T., 2011. Phosphorylcholine Phosphatase: a Peculiar Enzyme of *Pseudomonas aeruginosa*, vol. 2011. Enzyme Research.

Dubovenko, A.G., Dunaevsky, Y.E., Belozersky, M.A., Oppert, B., Lord, J.C., Elpidina, E. N., 2010. Trypsin-like proteins of the fungi as possible markers of pathogenicity. Fungal Biol. 114 (2–3), 151–159.

Dwivedi, R.C., Spicer, V., Harder, M., Antonovici, M., Ens, W., Standing, K.G., Wilkins, J. A., Krokhin, O.V., 2008. Practical implementation of 2D HPLC scheme with accurate peptide retention prediction in both dimensions for high-throughput bottom-up proteomics. Anal. Chem. 80 (18), 7036–7042.

El-Bebany, A.F., Rampitsch, C., Daayf, F., 2010. Proteomic analysis of the phytopathogenic soilborne fungus *Verticillium dahliae* reveals differential protein expression in isolates that differ in aggressiveness. Proteomics 10 (2), 289–303.

Ellwood, S.R., Syme, R.A., Moffat, C.S., Oliver, R.P., 2012. Evolution of three *Pyrenophora* cereal pathogens: recent divergence, speciation and evolution of non-coding DNA. Fungal Genet. Biol. 49 (10), 825–829.

Emanuelsson, O., Nielsen, H., Brunak, S., von Heijne, G., 2000. Predicting subcellular localization of proteins based on their N-terminal amino acid sequence. J. Mol. Biol. 300 (4), 1005–1016.

Fabre, F., Bormann, J., Urbach, S., Roche, S., Langin, T., Bonhomme, L., 2019. Unbalanced roles of fungal aggressiveness and host cultivars in the establishment of the Fusarium Head Blight in bread wheat. Front. Microbiol. 10, 2857.

Fellbrich, G., Romanski, A., Varet, A., Blume, B., Brunner, F., Engelhardt, S., Felix, G., Kemmerling, B., Krzymowska, M., Nürnberger, T., 2002. NPP1, a *Phytophthora*-associated trigger of plant defense in parsley and *Arabidopsis*. Plant J. 32 (3), 375–390.

Figueiredo, L., Santos, R.B., Figueiredo, A., 2021. Defense and offense strategies: the role of aspartic proteases in plant-pathogen interactions. Biology 10 (2), 75.

Fischer, M., Pleiss, J., 2003. The lipase engineering database: a navigation and analysis tool for protein families. Nucleic Acids Res. 31 (1), 319–321.

Franck, W.L., Gokce, E., Oh, Y., Muddiman, D.C., Dean, R.A., 2013. Temporal analysis of the *Magnaporthe oryzae* proteome during conidial germination and cyclic AMP (cAMP)-mediated appressorium formation. Mol. Cell. Proteomics 12 (8), 2249–2265.

Friis, P., Olsen, C.E., Møller, B.L., 1991. Toxin production in *Pyrenophora teres*, the ascomycete causing the net-spot blotch disease of barley (*Hordeum vulgare* L.). J. Biol. Chem. 266 (20), 13329–13335.

Fu, H., Chung, K.R., Liu, X., Li, H., 2020. Aaprb1, a subtilsin-like protease, required for autophagy and virulence of the tangerine pathotype of *Alternaria alternata*. Microbiol. Res. 240, 126537.

Gerlegiz, E.T., Karakaya, A., Çelik Oğuz, A., Mert, Z., Sayim, İ., Ergün, N., Aydoğan, S., 2014. Assessment of the seedling reactions of some hulless barley genotypes to *Drechslera teres* f. *maculata*. Selcuk J. Agric. Food Sci. 28 (2), 63–68.

Gilbert, N.M., Donlin, M.J., Gerik, K.J., Specht, C.A., Djordjevic, J.T., Wilson, C.F., Sorrell, T.C., Lodge, J.K., 2010. KRE genes are required for beta-1,6-glucan synthesis, maintenance of capsule architecture and cell wall protein anchoring in Cryptococcus neoformans. Mol. Microbiol. 76 (2), 517–534.

Giraldo, M.C., Dagdas, Y.F., Gupta, Y.K., Mentlak, T.A., Yi, M., Martinez-Rocha, A.L., Saitoh, H., Terauchi, R., Talbot, N.J., Valent, B., 2013. Two distinct secretion systems facilitate tissue invasion by the rice blast fungus *Magnaporthe oryzae*. Nat. Commun. 4, 1996. https://doi.org/10.1038/ncomms2996.

Godfrey, D., Böhlenius, H., Pedersen, C., Zhang, Z., Emmersen, J., Thordal-Christensen, H., 2010. Powdery mildew fungal effector candidates share N-terminal Y/F/WxC-motif. BMC Genom. 11, 317.

Gui, Y.J., Chen, J.Y., Zhang, D.D., Li, N.Y., Li, T.G., Zhang, W.Q., Wang, X.Y., Short, D.P. G., Li, L., Guo, W., Kong, Z.Q., Bao, Y.M., Subbarao, K.V., Dai, X.F., 2017. *Verticillium dahliae* manipulates plant immunity by glycoside hydrolase 12 proteins in conjunction with carbohydrate-binding module 1. Environ. Microbiol. 19 (5), 1914–1932.

Harris, P.V., Welner, D., McFarland, K.C., Re, E., Navarro Poulsen, J.C., Brown, K., Salbo, R., Ding, H., Vlasenko, E., Merino, S., Xu, F., Cherry, J., Larsen, S., Lo Leggio, L., 2010. Stimulation of lignocellulosic biomass hydrolysis by proteins of glycoside hydrolase family 61: structure and function of a large, enigmatic family. Biochemistry 49 (15), 3305–3316.

Havenga, M., Wingfield, B.D., Wingfield, M.J., et al., 2021. Genetic response to nitrogen starvation in the aggressive Eucalyptus foliar pathogen *Teratosphaeria destructans*. Curr. Genet. 67, 981–990. https://doi.org/10.1007/s00294-021-01208-w.

Horton, P., Park, K.J., Obayashi, T., Fujita, N., Harada, H., Adams-Collier, C.J., Nakai, K., 2007. WoLF PSORT: protein localization predictor. Nucleic Acids Res. 2007 (35), W585–W587. Web Server issue).

Ismail, I.A., Able, A.J., 2016. Secretome analysis of virulent *Pyrenophora teres* f. *teres* isolates. Proteomics 16 (20), 2625–2636.
Ismail, I.A., Able, A.J., 2017. Gene expression profiling of virulence-associated proteins in planta during net blotch disease of barley. Physiol. Mol. Plant Pathol. 98, 69–79.
Ismail, I.A., Godfrey, D, Able, A.J., et al., 2014. Proteomic analysis reveals the potential involvement of xylanase from *Pyrenophora teres* f. *teres* in net form net blotch disease of barley. Australas. Plant Pathol. 43, 715–726. https://doi.org/10.1007/s13313-014-0314-7.
Jalli, M., 2011. Sexual reproduction and soil tillage effects on virulence of *Pyrenophora teres* in Finland. Ann. Appl. Biol. 158 (1), 95–105.
Karakaya, A., Akyol, A., 2006. Determination of the seedling reactions of some Turkish barley cultivars to the net blotch. Plant Pathol. J. 5 (1), 113–114.
Kettles, G.J., Bayon, C., Sparks, C.A., Canning, G., Kanyuka, K., Rudd, J.J., 2018. Characterization of an antimicrobial and phytotoxic ribonuclease secreted by the fungal wheat pathogen *Zymoseptoria tritici*. New Phytol. 217 (1), 320–331.
Kilaru, S., Hoegger, P.J., Kues, U., 2006. The laccase multi-gene family in *Coprinopsis cinerea* has seventeen different members that divide into two distinct subfamilies. Curr. Genet. 50 (1), 45–60.
Kubicek, C.P., Starr, T.L., Glass, N.L., 2014. Plant cell wall-degrading enzymes and their secretion in plant-pathogenic fungi. Annu. Rev. Phytopathol. 52, 427–451.
Lalaoui, F., Halama, P., Dumortier, V., Paul, B., 2000. Cell wall-degrading enzymes produced *in vitro* by isolates of *Phaeosphaeria nodorum*. Plant Pathol. 49, 727–733.
Lartey, R.T., Caesar-TonThat, T.C., Caesar, A.J., Sainju, U.M., Evans, R.G., 2013. First report of spot form net blotch caused by *Pyrenophora teres* f. *maculata* on barley in the Mon-Dak area of the United States. Plant Dis. 97 (1), 143.
Letunic, I., Bork, P., 2016. Interactive tree of life (iTOL) v3: an online tool for the display and annotation of phylogenetic and other trees. Nucleic Acids Res. 44 (W1), W242–W245.
Lightfoot, D.J., Able, A.J., 2010. Growth of *Pyrenophora teres* in planta during barley net blotch disease. Australas. Plant Pathol. 39 (6).
Lin, S.Y., Okuda, S., Ikeda, K., Okuno, T., Takano, Y., 2012. LAC2 encoding a secreted laccase is involved in appressorial melanization and conidial pigmentation in *Colletotrichum orbiculare*. Mol. Plant Microbe Interact. 25 (12), 1552–1561.
Liu, Z., Ellwood, S.R., Oliver, R.P., Friesen, T.L., 2011. *Pyrenophora teres*: profile of an increasingly damaging barley pathogen. Mol. Plant Pathol. 12 (1), 1–19.
Liu, N., Cao, Z., Cao, K., Ma, S., Gong, X., Jia, H., Dai, D., Dong, J., 2018. Identification of laccase-like multicopper oxidases from the pathogenic fungus *Setosphaeria turcica* and their expression pattern during growth and infection. Eur. J. Plant Pathol. 153 (4), 1149–1163.
Liu, B., Stevens-Green, R., Johal, D., Buchanan, R., Geddes-McAlister, J., 2022. Fungal pathogens of cereal crops: proteomic insights into fungal pathogenesis, host defense, and resistance. J. Plant Physiol. 269, 153593.
Ma, Z., Song, T., Zhu, L., Ye, W., Wang, Y., Shao, Y., Dong, S., Zhang, Z., Dou, D., Zheng, X., Tyler, B.M., Wang, Y., 2015. A *Phytophthora sojae* glycoside hydrolase 12 protein is a major virulence factor during soybean infection and is recognized as a PAMP. Plant Cell 27 (7), 2057–2072.
Manning, V.A., Pandelova, I., Dhillon, B., Wilhelm, L.J., Goodwin, S.B., Berlin, A.M., Figueroa, M., Freitag, M., Hane, J.K., Henrissat, B., Holman, W.H., Kodira, C.D., Martin, J., Oliver, R.P., Robbertse, B., Schackwitz, W., Schwartz, D.C., Spatafora, J. W., Turgeon, B.G., Yandava, C., Young, S., Zhou, S., Zeng, Q., Grigoriev, I.V., Ma, L. J., Ciuffetti, L.M., 2013. Comparative genomics of a plant-pathogenic fungus, *Pyrenophora tritici-repentis*, reveals transduplication and the impact of repeat elements on pathogenicity and population divergence. G3 (Bethesda) 3 (1), 41–63.
Marchler-Bauer, A., Lu, S., Anderson, J.B., Chitsaz, F., Derbyshire, M.K., DeWeese-Scott, C., Fong, J.H., Geer, L.Y., Geer, R.C., Gonzales, N.R., Gwadz, M., Hurwitz, D.I., Jackson, J.D., Ke, Z., Lanczycki, C.J., Lu, F., Marchler, G.H., Mullokandov, M., Omelchenko, M.V., Robertson, C.L., et al., 2011. CDD: a Conserved Domain Database for the functional annotation of proteins. Nucleic Acids Res. 39 (Database issue), D225–D229.
Mathre, D.E., 1997. In: Mathre, D.E. (Ed.), Compendium of Barley Diseases. APS Press, Minnesota, p. 78.
International Barley Genome Sequencing Consortium, Mayer, K.F., Waugh, R., Brown, J. W., Schulman, A., Langridge, P., Platzer, M., Fincher, G.B., Muehlbauer, G.J., Sato, K., Close, T.J., Wise, R.P., Stein, N., 2012. A physical, genetic and functional sequence assembly of the barley genome. Nature 491 (7426), 711–716.
McLean, M.S., Martin, A., Gupta, S., Sutherland, M.W., Hollaway, G.J., Platz, G.J., 2014. Validation of a new spot form of net blotch differential set and evidence for hybridisation between the spot and net forms of net blotch in Australia. Australas. Plant Pathol. 43 (3), 223–233.
Meng, Y., Zeng, F., Hu, J., Li, P., Xiao, S., Zhou, L., Gong, J., Liu, Y., Hao, Z., Cao, Z., Dong, J., 2022. Novel factors contributing to fungal pathogenicity at early stages of *Setosphaeria turcica* infection. Mol. Plant Pathol. 23 (1), 32–44.
Métraux, J.-P., Jackson, R.W., Schnettler, E., Goldbach, R.W., 2009. Plant pathogens as suppressors of host defense. Adv. Bot. Res. 51, 39–89.
Muria-Gonzalez, M.J., Yeng, Y., Breen, S., Mead, O., Wang, C., Chooi, Y.H., Barrow, R.A., Solomon, P.S., 2020. Volatile molecules secreted by the wheat pathogen *Parastagonospora nodorum* are involved in development and phytotoxicity. Front. Microbiol. 11, 466.
Nelson, A., Elias, K., Arévalo Gardini, E., Darlington, L., Bailey, B., 1997. Genetic characterization by RAPD analysis of an emerging epidemic in Peru of Fusarium oxysporum f. sp. erythroxyli. Phytopathology 87, 1220–1225.
Nguyen, Q.B., Itoh, K., Van Vu, B., Tosa, Y., Nakayashiki, H., 2011. Simultaneous silencing of endo-beta-1,4 xylanase genes reveals their roles in the virulence of *Magnaporthe oryzae*. Mol. Microbiol. 81 (4), 1008–1019.
Nitsche, B.M., Jørgensen, T.R., Akeroyd, M., Meyer, V., Ram, A.F., 2012. The carbon starvation response of *Aspergillus niger* during submerged cultivation: insights from the transcriptome and secretome. BMC Genom. 13, 380.
Nukina, M., Ikeda, M., Sassa, T., 1980. Two new pyrenolides, fungal morphogenic substances produced by *Pyrenophora teres* (Diedicke) *Drechsler*. Agric. Biol. Chem. 44 (11), 2761–2762.
Oh, Y., Robertson, S.L., Parker, J., et al., 2017. Comparative proteomic analysis between nitrogen supplemented and starved conditions in *Magnaporthe oryzae*. Proteome Sci. 15, 20.
Oldach, K.H., Becker, D., Lorz, H., 2001. Heterologous expression of genes mediating enhanced fungal resistance in transgenic wheat. Mol. Plant Microbe Interact. 14, 832–838.
Ozketen, A.C., Andac-Ozketen, A., Dagvadorj, B., Demiralay, B., Akkaya, M.S., 2020. In-depth secretome analysis of *Puccinia striiformis* f. sp. *tritici* in infected wheat uncovers effector functions. Biosci. Rep. 40 (12).
Pan, S., Tang, L., Pan, X., Qi, L., Yang, J., 2021. A member of the glycoside hydrolase family 76 is involved in growth, conidiation, and virulence in rice blast fungus. Physiol. Mol. Plant Pathol. 113, 101587.
Paper, J.M., Scott-Craig, J.S., Adhikari, N.D., Cuomo, C.A., Walton, J.D., 2007. Comparative proteomics of extracellular proteins in vitro and in planta from the pathogenic fungus *Fusarium graminearum*. Proteomics 7 (17), 3171–3183.
Pariaud, B., Ravigné, V., Halkett, F., Goyeau, H., Carlier, J., Lannou, C., 2009. Aggressiveness and its role in the adaptation of plant pathogens. Plant Pathol. 58 (3), 409–424.
Pemberton, C.L., Salmond, G.P., 2004. The Nep1-like proteins-a growing family of microbial elicitors of plant necrosis. Mol. Plant Pathol. 5 (4), 353–359.
Pennington, H.G., Jones, R., Kwon, S., Bonciani, G., Thieron, H., Chandler, T., Luong, P., Morgan, S.N., Przydacz, M., Bozkurt, T., Bowden, S., Craze, M., Wallington, E.J., Garnett, J., Kwaaitaal, M., Panstruga, R., Cota, E., Spanu, P.D., 2019. The fungal ribonuclease-like effector protein CSEP0064/BEC1054 represses plant immunity and interferes with degradation of host ribosomal RNA. PLoS Pathog. 15 (3), e1007620.
Petersen, T.N., Brunak, S., von Heijne, G., Nielsen, H., 2011. SignalP 4.0: discriminating signal peptides from transmembrane regions. Nat. Methods 8 (10), 785–786.
Raffaele, S., Win, J., Cano, L.M., Kamoun, S., 2010. Analyses of genome architecture and gene expression reveal novel candidate virulence factors in the secretome of *Phytophthora infestans*. BMC Genom. 11, 637.
Rafiei, V., Velez, H., Tzelepis, G., 2021. The role of glycoside hydrolases in phytopathogenic fungi and oomycetes virulence. Int. J. Mol. Sci. 22 (17).
Rampitsch, C., Bykova, N.V., McCallum, B., Beimcik, E., Ens, W., 2006. Analysis of the wheat and *Puccinia triticina* (leaf rust) proteomes during a susceptible host-pathogen interaction. Proteomics 6 (6), 1897–1907.
Rampitsch, C., Day, J., Subramaniam, R., Walkowiak, S., 2013. Comparative secretome analysis of *Fusarium graminearum* and two of its non-pathogenic mutants upon deoxynivalenol induction *in vitro*. Proteomics 13 (12–13), 1913–1921.
Rampitsch, C., Huang, M., Djuric-Cignaovic, S., Wang, X., Fernando, U., 2019. Temporal quantitative changes in the resistant and susceptible wheat leaf apoplastic proteome during infection by wheat leaf rust (*Puccinia triticina*). Front. Plant Sci. 1291.
Rau, D., Attene, G., Brown, A.H., Nanni, L., Maier, F.J., Balmas, V., Saba, E., Schafer, W., Papa, R., 2007. Phylogeny and evolution of mating-type genes from *Pyrenophora teres*, the causal agent of barley "net blotch" disease. Curr. Genet. 51 (6), 377–392.
Rudolph, J.D., Cox, J., 2019. A network module for the Perseus Software for computational proteomics facilitates proteome interaction graph analysis. J. Proteome Res. 18 (5), 2052–2064.
Saei, A.A., Beusch, C.M., Chernobrovkin, A., et al., 2019. ProTargetMiner as a proteome signature library of anticancer molecules for functional discovery. Nat. Commun. 10, 5715.
Sarpeleh, A., Wallwork, H., Catcheside, D.E., Tate, M.E., Able, A.J., 2007. Proteinaceous metabolites from *Pyrenophora teres* contribute to symptom development of barley net blotch. Phytopathology 97 (8), 907–915.
Saunders, D.G., Win, J., Cano, L.M., Szabo, L.J., Kamoun, S., Raffaele, S., 2012. Using hierarchical clustering of secreted protein families to classify and rank candidate effectors of rust fungi. PLoS One 7 (1), e29847.
Sievers, F., Wilm, A., Dineen, D., Gibson, T.J., Karplus, K., Li, W., Lopez, R., McWilliam, H., Remmert, M., Söding, J., Thompson, J.D., Higgins, D.G., 2011. Fast, scalable generation of high-quality protein multiple sequence alignments using Clustal Omega. Mol. Syst. Biol. 7, 539.
Smedegård-Petersen, V., 1977. Inheritance of genetic factors for symptoms and pathogenicity in hybrids of *Pyrenophora teres* and *Pyrenophora graminea*. J. Phytopathol. 89 (3), 193–202.
Smith, P.K., Krohn, R.I., Hermanson, G.T., Mallia, A.K., Gartner, F.H., Provenzano, M.D., Fujimoto, E.K., Goeke, N.M., Olson, B.J., Klenk, D.C., 1985. Measurement of protein using bicinchoninic acid. Anal. Biochem. 150 (1), 76–85.
Soliman, A., Rampitsch, C., Tambong, J.T., Daayf, F., 2021. Secretome analysis of *Clavibacter nebraskensis* strains treated with natural xylem sap in vitro predicts involvement of glycosyl hydrolases and proteases in bacterial aggressiveness. Proteomes 9, 1.
Sperschneider, J., Gardiner, D.M., Taylor, J.M., Hane, J.K., Singh, K.B., Manners, J.M., 2013. A comparative hidden Markov model analysis pipeline identifies proteins characteristic of cereal-infecting fungi. BMC Genom. 14 (1), 1–23.
Sperschneider, J., Catanzariti, A.M., Deboer, K., Petre, B., Gardiner, D.M., Singh, K.B., Dodds, P.N., Taylor, J.M., 2017. Localizer: subcellular localization prediction of both plant and effector proteins in the plant cell. Sci. Rep. 7, 44598.
Sperschneider, J., Dodds, P.N., Gardiner, D.M., Singh, K.B., Taylor, J.M., 2018. Improved prediction of fungal effector proteins from secretomes with EffectorP 2.0. Mol. Plant Pathol. 19 (9), 2094–2110.

Syme, R.A., Martin, A., Wyatt, N.A., Lawrence, J.A., Muria-Gonzalez, M.J., Friesen, T.L., Ellwood, S.R., 2018. Transposable element genomic fissuring in *Pyrenophora teres* is associated with genome expansion and dynamics of host–pathogen genetic interactions. Front. Genet. 9, 130.

Talbot, N.J., 2003. On the trail of a cereal killer: exploring the biology of *Magnaporthe grisea*. Annu. Rev. Microbiol. 57, 177–202.

Tekauz, A., 1985. A numerical scale to classify reactions of barley to *Pyrenophora teres*. J. Indian Dent. Assoc. 7 (2), 181–183.

Torregrosa, C., Cluzet, S., Fournier, J., Huguet, T., Gamas, P., Prospéri, J.-M., Esquerré-Tugayé, M.-T., Dumas, B., Jacquet, C., 2004. Cytological, genetic, and molecular analysis to characterize compatible and incompatible interactions between *Medicago truncatula* and *Colletotrichum trifolii*. Mol. Plant Microbe Interact. 17, 909–920.

Toruño, T.Y., Stergiopoulos, I., Coaker, G., 2016. Plant-pathogen effectors: cellular probes interfering with plant defenses in spatial and temporal manners. Annu. Rev. Phytopathol. 54, 419–441.

Tyanova, S., Temu, T., Cox, J., 2016. The MaxQuant computational platform for mass spectrometry-based shotgun proteomics. Nat. Protoc. 11 (12), 2301–2319.

Usta, P., Karakaya, A., Çelik Oğuz, A., Mert, Z., Akan, K., Çetin, L., 2014. Determination of the seedling reactions of twenty barley cultivars to six isolates of *Drechslera teres* f. *maculata*. Anadolu J. Agric. Sci. 29 (1), 20–25.

Van Vu, B., Itoh, K., Nguyen, Q.B., Tosa, Y., Nakayashiki, H., 2012. Cellulases belonging to glycoside hydrolase families 6 and 7 contribute to the virulence of *Magnaporthe oryzae*. Mol. Plant Microbe Interact. 25 (9), 1135–1141.

Wang, Y., Wu, J., Park, Z.Y., Kim, S.G., Rakwal, R., Agrawal, G.K., Kim, S.T., Kang, K.Y., 2011. Comparative secretome investigation of *Magnaporthe oryzae* proteins responsive to nitrogen starvation. J. Proteome Res. 10 (7), 3136–3148.

Wang, X., Mace, E.S., Platz, G.J., Hunt, C.H., Hickey, L.T., Franckowiak, J.D., Jordan, D. R., 2015. Spot form of net blotch resistance in barley is under complex genetic control. Theor. Appl. Genet. 128 (3), 489–499.

Wei, J., Cui, L., Zhang, N., Du, D., Meng, Q., Yan, H., Liu, D., Yang, W., 2020. *Puccinia triticina* pathotypes THTT and THTS display complex transcript profiles on wheat cultivar Thatcher. BMC Genet. 21 (1), 48.

Wyatt, N.A., Friesen, T.L., 2021. Four reference quality genome assemblies of *Pyrenophora teres* f. *maculata*: a resource for studying the barley spot form net blotch interaction. Mol. Plant Microbe Interact. 34 (1), 135–139.

Wyatt, N.A., Richards, J.K., Brueggeman, R.S., Friesen, T.L., 2018. Reference assembly and annotation of the *Pyrenophora teres* f. *teres* Isolate 0-1. G3 (Bethesda) 8 (1), 1–8.

Yang, B., Wang, Y., Tian, M., Dai, K., Zheng, W., Liu, Z., Yang, S., Liu, X., Shi, D., Zhang, H., Wang, Y., Ye, W., Wang, Y., 2021. Fg12 ribonuclease secretion contributes to *Fusarium graminearum* virulence and induces plant cell death. J. Integr. Plant Biol. 63 (2), 365–377.

Zadoks, J.C., Chang, T.T., Konzak, C.F., 1974. A decimal code for the growth stages of cereals. Weed Res. 14, 415–421.

Zhang, S., Xu, J.R., 2014. Effectors and effector delivery in *Magnaporthe oryzae*. PLoS Pathog. 10 (1), e1003826.

Zhao, Z., Liu, H., Wang, C., Xu, J.R., 2014. Correction: comparative analysis of fungal genomes reveals different plant cell wall degrading capacity in fungi. BMC Genom. 15, 6.

Zhao, Q., Ding, Y., Song, X., Liu, S., Li, M., Li, R., Ruan, H., 2021. Proteomic analysis reveals that naturally produced citral can significantly disturb physiological and metabolic processes in the rice blast fungus *Magnaporthe oryzae*. Pestic. Biochem. Physiol. 175, 104835.